MECHANICAL PROPERTY MEASUREMENT OF 0.5-μm CMOS MICROSTRUCTURES

M. S.-C. LU *, X. ZHU *, G. K. FEDDER **
* ECE Department, Carnegie Mellon University, PA 15213, mslu@ece.cmu.edu
**ECE Department and the Robotics Institute, Carnegie Mellon University, PA 15213

ABSTRACT

Measurements are reported on the mechanical properties of high-aspect-ratio micromechanical structures formed using a conventional 0.5-μm CMOS process. Composite structures are etched out of the CMOS dielectric, aluminum, and gate-polysilicon thin films using a post-CMOS CHF_3:O_2 reactive-ion etch and followed by a SF_6:O_2 silicon etch for release. Microstructures have a height of 5 μm and beam widths and gaps down to 1.2 μm. Properties are strongly dependent on the relative metal and dielectric content of the beams. Beams with three metal conductors and polysilicon have an effective Young's modulus of 62 GPa, residual stress of -29 MPa, and an average out-of-plane radius of curvature of 1.9 mm. Maximum Young's modulus variation is 3 GPa die-to-die, and is 9 GPa between two runs. Die-to-die variation of stress and stress gradient is poor for many beam compositions, however local matching on a die is very good. Cracking is induced in a resonant fatigue structure at 620 MPa of repetitive stress after over 50 million cycles.

INTRODUCTION

Building microelectromechanical systems (MEMS) in conventional CMOS processes has many potential advantages. Integration of high-performance electronics with microstructures involves only incremental processing after the CMOS is completed, thereby enabling a shift in research focus from processing details to the design of complex systems with multiple sensors and actuators on a single chip. The base CMOS fabrication is inexpensive, fast, reliable, and available from external foundries.

Several kinds of CMOS MEMS processing have been developed to meet a variety of application needs [2][3][4]. A common process uses stacked vias in the CMOS followed by a wet silicon undercut etch to create thermomechanical structures [5]. Microstructures are made from combinations of oxide, aluminum, and polysilicon thin films. The metallization and dielectric layers serve a dual function as electrical interconnect and structural material. The gate polysilicon is often used in thermal heater resistors, piezoresistive sensors, and thermopiles. General mechanical and thermal properties of CMOS-MEMS have been reported [6][7].

High-aspect-ratio CMOS-MEMS are created by placing the critical structural sidewall etching step after completion of the CMOS, thereby decoupling issues involving the microstructural sidewall geometry from the CMOS process [1]. Beams of widths from 1.2 μm to 15 μm can be released with gap spacings down to 1.2 μm. The availability of narrow beam widths and gaps provides increased design flexibility. The process is a potentially attractive alternative to polysilicon micromachining for manufacture of resonant sensors, accelerometers, and vibratory-rate gyroscopes. However, a current bottleneck in successful design is the lack of characterization data on the material properties of the micromechanical structures.

In this paper, we present the first set of mechanical property data for high-aspect-ratio CMOS microstructures. Experimental measurements of effective Young's modulus, residual stress and vertical stress gradient showing die-to-die and run-to-run variations are presented. An initial test of durability is performed on a resonating fatigue structure which demonstrates the effects of cyclic stress on composite micromechanical structures.

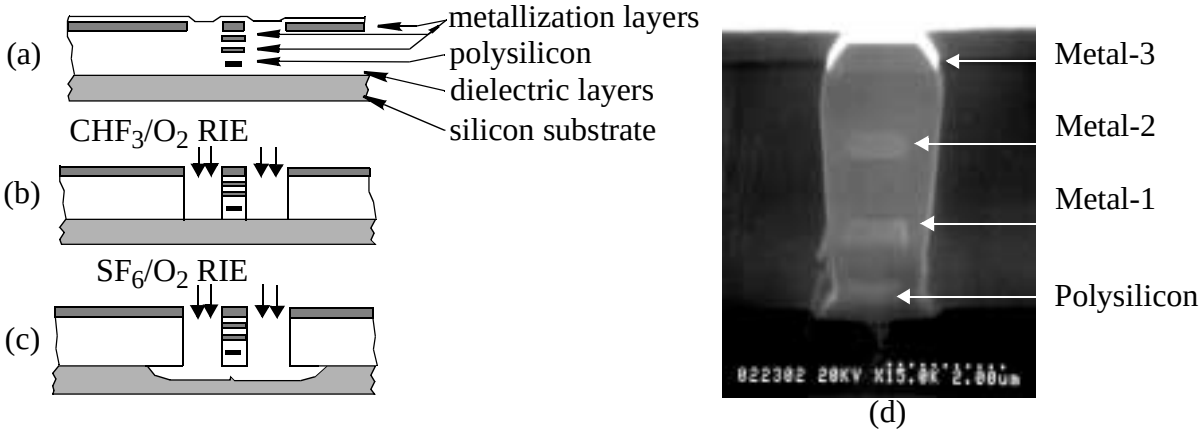

Figure 1. Cross sections of the high-aspect-ratio CMOS-MEMS process flow. (a) After CMOS processing. (b) After dielectric reactive-ion etch for definition of structural sidewalls. (c) After isotropic silicon etch for structural release. (d) SEM of a m3-m2-m1-poly beam.

FABRICATION

Structures are made using the Hewlett-Packard 0.5 μm three-metal n-well CMOS process available through the MOS Implementation Service (MOSIS). The microstructure is defined after completion of the CMOS processing by two reactive-ion etching (RIE) steps, as illustrated in Figure 1, using a Plasma-Therm 790 Etcher. First, a CHF_3/O_2 anisotropic etch of the dielectric layers defines the structural sidewalls (Figure 1(b)). The top metal interconnection layer is used as an etch-resistant mask for the microstructure definition. Next, a nearly isotropic SF_6/O_2 etch undercuts the silicon substrate and releases the structure (Figure 1(c)). The scanning electron micrograph (SEM) in Figure 1(d) is of a released composite beam with three metal conductors and polysilicon. The three metal layers from top to bottom are abbreviated m3, m2, and m1. At most fourteen different composite structures can be made by using different combinations of the embedded metal layers and polysilicon.

The dielectric etch settings are critical and require a compromise between reasonable etch rate, structural profile, loss of critical dimension, polymer generalization, and survival of electrical via connections. By conducting a Box-Behnken [8] 3-factor design to analyze the effects of pressure, power and different gas flow ratio, a suitable processing recipe for dielectric etching was obtained. The process settings are gas flows of 22.5 sccm CHF_3 and 16.0 sccm O_2, pressure of 125 mTorr, and power of 100 W. From our observation, this processing recipe is not very sensitive to the composition of the dielectrics (e.g., etch rates are similar for the intermetal oxide and field oxide). The statistical analysis for the etch rate on MOSIS N7BH-AV and N79V-AQ runs is 424$\mathring{A}$/min over 48 dice with a standard deviation of ±6%. The etch rate of silicon is under characterization, with initial vertical-to-lateral Si etch rates of 1.5:1 to 2.5:1.

EXPERIMENTAL MEASUREMENT

Effective Young's Modulus

Effective Young's modulus is determined by optically measuring the lateral resonance frequency of simple cantilever beams. Small electrostatic actuators located near the tips of the cantilevers provide the actuation force. The measured values are substituted into the analytic equation for resonance frequency of a homogeneous cantilever beam, $f_r = 0.56\sqrt{EI/mL^4}$, where L is the

Table I: Effective Young's modulus in GPa of composite beams measured from MOSIS N78H-AV run

m3	m2	m1	poly	die no.1	die no.2	die no.3	Average	standard deviation	volume (dielectric : metal)
•	•	•	•	63 ± 0.4	62 ± 0.4	61 ± 0.4	62.0	0.82	4.02 : 1
•	•	•		64 ± 0.4	62 ± 0.4	60 ± 0.4	62.0	1.63	4.15 : 1
•	•		•	73 ± 0.4	69 ± 0.4	67 ± 0.4	69.7	2.49	5.77 : 1
•	•			73 ± 0.4	71 ± 0.4	67 ± 0.4	70.3	2.49	5.95 : 1
•		•	•	73 ± 0.4	71 ± 0.4	66 ± 0.4	70.3	2.94	5.77 : 1
•		•		74 ± 0.4	71 ± 0.4	69 ± 0.4	71.3	2.05	5.95 : 1
•			•	82 ± 0.4	80 ± 0.4	75 ± 0.4	79.0	2.94	9.39 : 1
•				83 ± 0.4	80 ± 0.4	77 ± 0.4	80.0	2.45	9.67 : 1
	•	•	•	67 ± 0.3	N/A	65 ± 0.3	66.0	1.00	5.28 : 1
	•	•		67 ± 0.3	66 ± 0.3	N/A	66.5	0.50	5.50 : 1
	•		•	78 ±0.3	75 ± 0.3	75 ± 0.3	76.0	1.41	10.10 : 1
	•			77 ± 0.3	78 ± 0.3	79 ± 0.3	78.0	0.82	10.50 : 1
		•	•	N/A	66 ± 0.3	67 ± 0.3	66.5	0.50	4.92 : 1
		•		N/A	67 ± 0.3	67 ± 0.3	67.0	0.00	5.35 : 1

Table II: Effective Young's modulus in GPa measured from N6CJ-AV and N78H-AV runs

m3	m2	m1	poly	N6CJ-AY					N78H-AV Average
				die no.1	die no.2	die no.3	Average	standard deviation	
•	•	•	•	65 ± 0.5	63 ± 0.5	62 ± 0.5	63.3	1.25	62.0
•	•	•		66 ± 0.5	65 ± 0.5	64 ± 0.5	65.0	0.82	62.0
•	•			74 ± 0.5	70 ± 0.5	70 ± 0.5	71.3	1.89	70.3
•		•		75 ± 0.5	71 ± 0.5	71 ± 0.5	72.3	2.16	71.3
•				89 ± 0.4	88 ± 0.4	91 ± 0.4	89.3	1.25	80.0

beam length, *E* is the effective Young's modulus, *I* is the moment of inertia of the beam cross-section, and *m* is the mass per unit length. Electrostatic spring softening is very small and is neglected.

Fourteen different kinds of composite beams were measured. Each cantilever was 2.1 μm wide and 90 μm long in layout. The actual dimensions of the beam cross-sections were measured from scanning electron micrographs. Table I summarizes the effective Young's modulus calculated from three dice from the MOSIS N78H-AV run. Resonance measurements have a ± 500 Hz uncertainty. The volume ratio of dielectric to metal in the right column illustrates that effective Young's modulus tends to increase when structures contain more dielectric than metal. Table II lists the effective Young's modulus of five composite beams from three dice on the MOSIS N6CJ-AY run, and the average result from the N78H-AV run for comparison. Both die-to-die and run-to-run variation of Young's modulus are within ± 8%, and within ± 3% for m3-m2-m1-poly beams.

Residual Stress and Vertical Stress Gradient

Residual stress is measured using bent-beam strain sensors [9], as shown in Figure 2 (a). Rel-

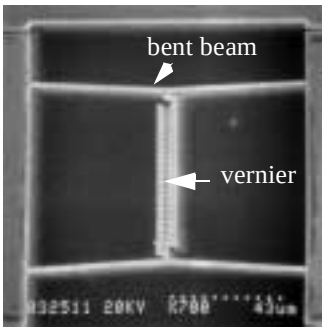

(a)

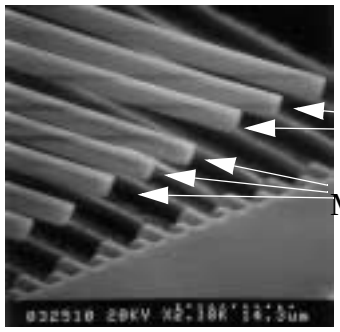

(b)

Figure 2. (a) SEM of a bent-beam strain sensor [9]. (b) SEM showing the matched out-of-plane curling for identical beams placed close together on the same die.

Table III: Residual stress in MPa measured from three separate runs.

m3	m2	m1	poly	Run N78Q-AH		Run N79V-AQ		Run N78H-AV		Average and standard deviation
				die no.1	die no2	die no.1	die no.2	die no.1	die no.2	
•	•	•	•	–28±2	–23±2	–28±2	–34±2	–29±2	–33±2	–29.2/3.62
•	•	•		–43±2	–43±2	–43±2	–43±2	–42±2	–43±2	–42.8/0.37
•	•			–70±2	–65±2	–72±2	–72±2	–74±2	–72±2	–70.8/2.85
•				–100±2	–100±2	–100±2	–116±2	–100±2	–100±2	–102.7/5.96
	•	•		–64±2	–74±2	–52±2	–50±2	–59±2	–61±2	–59.7/7.36
	•			–105±2	–105±2	–88±2	–70±2	–96±2	–98±2	–93.1/12.1
		•		–66±2	–66±2	–44±2	–44±2	–53±2	–53±2	–53.3/9.03

ative apex displacement of the bent-beam rendered by the residual stress is read out from a vernier.

Residual stress of seven composite test structures was analyzed by finite element modeling (FEM) using MEMCAD [10]. Stress was introduced in the model as $\sigma = E\Delta_T\alpha$ using the standard technique of applying an equivalent temperature change, Δ_T, and equivalent thermal expansion coefficient, α. Table III summarizes the results of residual stress from dice of N78Q-AH, N79V-AQ, and N78H-AV runs. Similar to the observations of effective Young's modulus, residual stress tends to increase when structures have increasing dielectric content. Beams containing all four conductors have relatively low compressive stress and variation of 20%.

Curling of the structural material arises from the residual vertical stress gradient in the composite structures. Figure 2(b) shows the uniform curl of several identical beams on one die. Table IV summarizes the measured out-of-plane radius of curvature of various 100 μm long, 2.1 μm wide composite beams from dice of N78Q-AH, N79V-AQ, and N78H-AV runs. The composite materials often exhibit substantial variation in stress gradient from die to die and run to run.

Cyclic Fatigue

Cyclic fatigue of the CMOS microstructures was investigated by using a modified fatigue structure obtained from Failure Analysis Associates, Inc. [11], as shown in Figure 3(a). Stress concentration induced by cyclic motion near the notch at the base of the structure gives rise to the fatigue crack growth, and causes the failure of the structure.

Resonance frequency of the structure was first measured at 13.1 kHz with a spectrum analyzer, as shown in Figure 3 (b). The lower peak shown is an out-of-plane mode excited from pull-down forces generated by the upward curling comb-finger electrodes. A durability test was done by driv-

Table IV: Radius of curvatures in mm measured from dice of N78Q-AH, N79V-AQ, and N78H-AV runs.

m3	m2	m1	poly	N78Q-AH		N79V-AQ		N78H-AV		Average and standard deviation
				die no.1	die no.2	die no.1	die no.2	die no.1	die no.2	
•	•	•	•	2.5	1.7	2.7	1.7	0.9	1.7	1.86 / 0.59
•	•	•		1.7	1.3	1.0	1.7	1.0	1.5	1.37 / 0.29
•	•		•	1.7	1.7	1.7	10.0	0.9	1.3	2.88 / 3.20
•	•			1.0	1.1	1.1	1.1	1.0	0.8	1.02 / 0.11
•		•	•	10.0	10.0	1.3	10.0	0.9	1.7	5.65 / 4.36
•		•		10.0	10.0	1.5	3.5	0.8	1.7	4.48 / 3.92
•			•	5.4	10.0	1.3	10.0	1.0	1.3	4.83 / 3.94
•				5.4	1.3	1.3	1.3	1.3	1.0	1.93 / 1.55
	•	•	•	1.7	1.3	0.8	0.9	1.0	0.6	1.05 / 0.36
	•	•		0.7	0.6	0.7	0.7	0.6	0.6	0.65 / 0.05
	•		•	0.7	0.7	0.8	0.9	0.7	0.7	0.75 / 0.08
	•			0.7	0.7	0.8	0.7	0.8	0.7	0.73 / 0.05

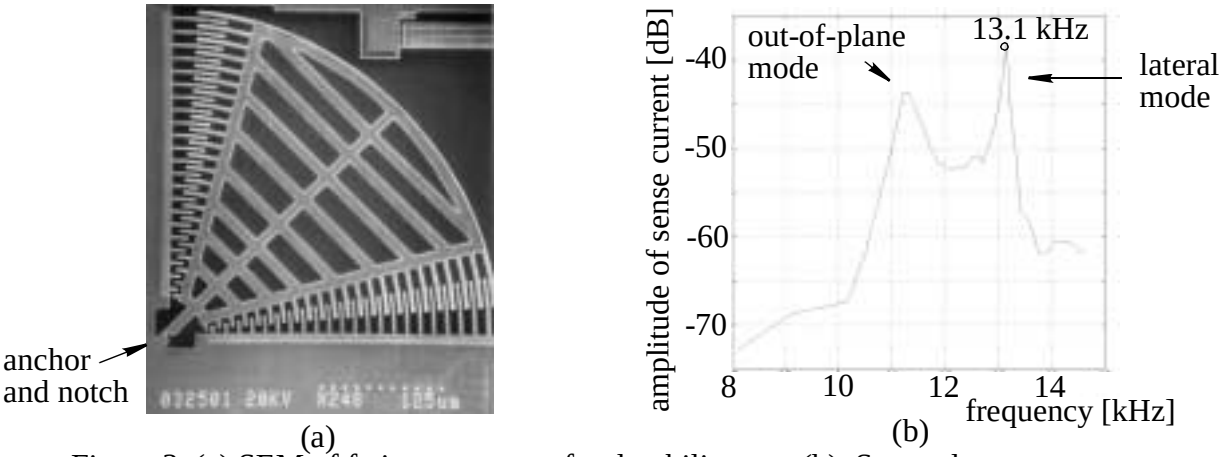

Figure 3. (a) SEM of fatigue structure for durability test. (b). Spectral response.

ing the structure at 40 V a.c. while biased at 55 V d.c., obtaining a maximum deflection of 10 ± 1 μm measured at the free end of the structure. Failure of the notch was observed after 72 minutes and over 45 million cycles. Figure 4(a) shows the change in resonance frequency with respect to the experienced cycles. Scanning electron micrographs of the notch taken before and after the excitation are shown in Figure 4 (b) and (c). The maximum stress value near the notch of 620 ± 60 MPa was obtained by finite element analysis using the measured end deflection of 10 μm.

CONCLUSION

Post-etching parameters of high-aspect-ratio CMOS-MEMS structures have been investigated through a factorial experiment analysis to enable consistent fabrication of microstructures. Material property measurements provide critical information for design of laterally actuated CMOS-MEMS. Effective Young's modulus varies within 8% and residual stress varies within 20% between runs, which enables designers to avoid buckling from compressive stress and to make consistent working devices. Vertical stress gradient is much more sensitive to both foundry and post-

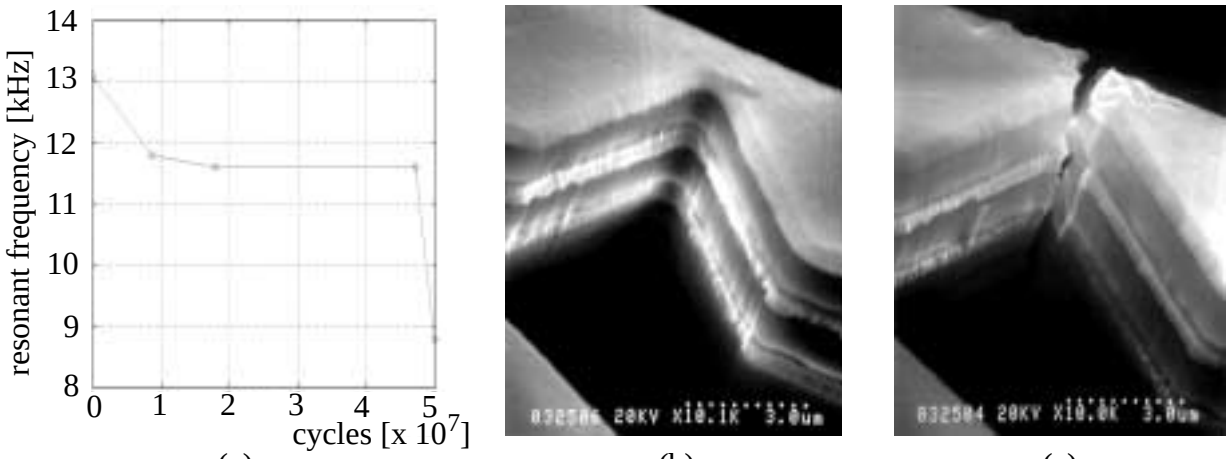

Figure 4. (a) Frequency change of the fatigue structure with respect to the experienced cycles. (b)Side view of the notch before testing. (c) After testing.

processing variations. However, curling of structures which are close to each other matches to within the measurement resolution of the SEM. Matched cantilevered structures may be designed to reduce effects of manufacturing variations in strain gradient. Preliminary results of a fatigue structure subjected to cyclic stress illustrates the start of a future research direction towards reliability issues of CMOS-MEMS structures.

ACKNOWLEDGMENTS

The authors thank William Tang and Russell Lawton of the Jet Propulsion Laboratory for FIB analysis and Chris Muhlstein of Failure Analysis Associates for discussions and use of their fatigue structure design. The research effort was sponsored by JPL and by DARPA under the AFOSR, Air Force Materiel Command, USAF, under cooperative agreement F30602-96-2-0304.

REFERENCE

1. G. K. Fedder, S. Santhanam, M. L. Reed, S. C. Eagle, D. F. Guillou, M. S.-C. Lu, and L. R. Carley, Sensors and Actuators A, 57, pp. 103-110 (1996).
2. M. Biebl, T. Scheiter, C. Hierold, H. V. Philipsborn and H. Klose, Sensors and Actuators A, 46-47, pp. 593-597 (1995).
3. H. Seidel, U. Fritsch, R. Gottinger, J. Schalk, J. Walter and K. Ambaum, Tech. Digest, 8th Int. Conf. Solid-State Sensors and Actuators (Transducers '95)/Eurosensors IX, Stockholm, Sweden, Vol. 1, pp. 597-600 (1995).
4. E. Hoffman, B. Warneka, E. Kruglick, J. Weigold and K. S. J. Pister, Proc. IEEE Micro Electro Mech. Syst. Workshop, Amsterdam, Netherlands, pp. 288-293 (1995).
5. M. Parameswaran, H.P. Baltes, L. Ristic, A. C. Dhaded and A. M. Robinson, Sensors and Actuators A, 19, pp. 289-307 (1989).
6. B. C. Read, III, V. M. Bright and J. H. Comtois, Proc. SPIE - Int. Soc. Opt. Eng. (USA), Vol. 2642, pp. 22-32 (1995).
7. O. M. Paul, J. Korvink and H. Baltes, Sensors and Actuators A, 41, pp. 161-164 (1994).
8. G. R. Bryce and D. Collette, Microelectronics Manufacturing and Testing, p.25 (Oct. 1984).
9. Y. B. Gianchandani and K. Najafi, IEEE J. MEMS, 5, pp. 52-58 (1996).
10. MEMCAD 3.2 User Guide, Microcosm Technologies, Inc.
11. S. B. Brown and E. Janson, Digest. IEEE/LEOS 1996 Summer Topical Meetings, Optical MEMS and their applications, pp. 9-10.